Contribution to the search for binaries among Am stars. VI. Orbital elements of ten new spectroscopic binaries, implications on tidal effects

Jean-Michel Carquillat, Jean-Louis Prieur, Nicole Ginestet, Edouard Oblak, Maria Kurpinska-Winiarska

Mon. Not. R. Astron. Soc. **000**, 000–000 (0000) Printed 11 February 2004 (MN LATEX style file v1.4)

Contribution to the search for binaries among Am stars.
VI. Orbital elements of ten new spectroscopic binaries.

J.-M. Carquillat,[1] J.-L. Prieur,[1] N. Ginestet,[1]
E. Oblak,[2] M. Kurpinska-Winiarska,[3]

[1] *UMR 5572 d'Astrophysique, Observatoire Midi-Pyrénées – CNRS, 14, Avenue Edouard Belin, 31400 Toulouse, France.*

[2] *UMR 6091, Observatoire de Besançon – CNRS, 41bis avenue de l'observatoire, 25010 Besançon, France.*

[3] *Obserwatorium Astronomiczne, Uniwersytet Jagiellonski, 171 ulica Orla, 30244 Krakow, Poland.*

Received 11 February 2004; accepted

ABSTRACT

We present the results of a radial-velocity study of ten Am stars (HD 19342, 19910, 36360, 102925, 126031, 127263, 138406, 155714, 195692 and 199360) observed at Observatoire de Haute-Provence with the CORAVEL instrument. We find that these systems are spectroscopic binaries whose orbital elements are determined for the first time. Both components were measured for HD 126031, an eclipsing binary, whereas the other systems were detected as single-line binaries only. Physical parameters were inferred from this study for the primaries of all systems, and for the secondary of HD 126031. We observed a higher rate of synchronized/circularized systems than expected from the theoretical models of radiative dissipation of dynamical tides.

Key words: Binaries: spectroscopic — Stars: fundamental parameters

1 INTRODUCTION

This paper is the sixth of a series devoted to the search and study of spectroscopic binaries (SB) among a sample of chemically peculiar stars of type Am. A presentation about the earlier papers of this series was given in the last one (Carquillat et al. 2003, paper V). A forthcoming paper will deal with statistics about the whole programme.

We present here the results of a radial velocity (RV) monitoring of ten such stars, namely HD 19342, 19910, 36360, 102925, 126031, 127263, 138406, 155714, 195692 and 199360. Most of the observations were carried out with the CORAVEL instrument of the 1-m Swiss telescope at Haute-Provence Observatory (OHP) and that of the 91 cm telescope of Cambridge Observatory. All those stars were detected as single-lined spectroscopic binaries (SB1) with CORAVEL. We thus could determine for the first time (to our knowledge) their orbital elements. For the eclipsing binary HD 126031, complementary observations with the 1.93 m telescope at OHP allowed us to detect the secondary component.

Six stars of the present sample come from the *"Third catalogue of Am stars with known spectral types"* (Hauck 1986, hereafter HCK86), and four from the list of Bidelman (1988) (hereafter BID88) entitled *"Miscellaneous spectroscopic notes"*. Only for 5 objects was the variability of the radial velocity already mentioned in previous studies. In Section 2, we present the RV observations and the orbital elements we computed. In Section 3 we give some complementary bibliographical information for each system. In Section 4 we derive some physical parameters deduced from available Strömgren photometry, Hipparcos parallaxes and theoretical evolutionary tracks (Sect. 4.2). We also estimate the minimum masses and separations of the companions (Sect. 4.3). We present an analysis of the Hipparcos light-curve of the eclipsing binary HD 126031 in Sect. 4.4. In Sect. 4.6, we compare our results with some theoretical predictions about the circularization of the orbits caused by tidal effects. Finally, using the projected rotational velocity $v \sin i$ derived from the correlation dips, we discuss the occurrence of rotation–revolution synchronism among those systems (Sect. 4.7).

2 OBSERVATIONS AND DERIVATION OF ORBITAL ELEMENTS

Our observations were performed in three-fold parts:

- J.-M. Carquillat and N. Ginestet first observed at OHP during the 1992–1998 period, with the CORAVEL instrument mounted on the 1-m Swiss telescope.
- In 2001–2002, E. Oblak and M. Kurpinska-Winiarska performed radial velocity measurements of HD 126031 on the 1.93-m at OHP, with the ELODIE spectrograph (Baranne et al., 1996).
- Finally in 2003, R.F. Griffin kindly made measurements with his own CORAVEL on the 91-cm telescope of Cambridge observatory.

Let us recall that CORAVEL is a spectrophotometer that allows measurements of heliocentric RVs by performing a cross-correlation of the stellar spectrum with a physical mask placed in the focal plane of the spectrograph (Baranne, Mayor & Poncet 1979). Although CORAVEL was designed to be efficient for observing cool stars, with a spectral type later than F4, it happens that many Am stars, which rotate slowly and present a spectrum with numerous sharp metallic features, are also suitable for producing a correlation dip.

For each star, between 30 and 50 RVs were obtained (Tables 1 to 10) with a mean internal standard error that depends upon the depth and the width of the correlation dip. The latter is strongly correlated with the rotational velocity $v \sin i$. The best precision was reached for HD 19342 (0.4 km.s^{-1}), the poorest for HD 195692 (1.3 km.s^{-1}), while eight stars have RVs errors in the range 0.4—0.8 km.s^{-1}. The RVs obtained at Cambridge are marked with the symbol ^{C} in the Tables 2, 5 and 6. All those RVs were reduced to the RV data base system of Geneva Observatory (Udry, Mayor & Queloz 1999), via the application of appropriate offsets.

For HD 155714 we added 4 RVs published by Nordström et al. (1997) (marked with the symbol ^{N} in Table 8), derived from the cross-correlation of digitized spectra with optimized synthetic template spectra. Taking into account the errors, those RVs were weighted 0.55 (whereas we used 1.0 for the CORAVEL measures).

For HD 126031, the ELODIE RVs (marked with the symbol ^{E} in Table 5) were weighted 2.0, to take into account their better quality than the CORAVEL data (weighted as 1.0). The small values of the internal errors given by ELODIE ($\sim$0.1 km.s^{-1}) would suggest larger values for the weights. Nevertheless, as the corresponding observations were concentrated in a short period of time, using larger weights for the ELODIE data degraded the accuracy of most parameters of the orbit (in particular P and T_0).

We calculated the spectroscopic orbital elements of the binaries (Tables 11 and 12) by applying the least-squares programs BS1 and BS2 (first created by Nadal et al. 1979 and revised by JLP) to the observed RVs. The $(O - C)$ residuals are given in Tables 1 to 10, and the computed RV curves in Figs 1 and 2. In all cases, the standard deviation of the residuals, $\sigma_{(O-C)}$, is consistent with the RV mean error (and even smaller, in the case of 7 objects), which indicates the absence of detectable spectroscopic third components in those systems.

The application of Lucy & Sweeney's (1971) statistical test to the orbital elements showed that six systems have a circular orbit: HD 19342, 102925, 126031, 155714, 195692, and 199360. The periods of HD 102925 (P = 16.4 days) and HD 19342 (P = 42.6 days) seem

rather large for the orbit to be circularized by tidal effects. We shall discuss that topic in Sect. 4.6.

3 NOTES FOR INDIVIDUAL SYSTEMS

In this section, we report some information about the studied stars and, in particular, the source for the Am classification (HCK86, BID88 or Grenier et al. (1999), hereafter GRE99) with, when available, the classifications from Ca II K line (k), hydrogen lines (h) and metallic lines (m).

HD 19342. HCK86 gives A7(k) F0(m) according to Walther (1949) and A5(k) F2(m) according to Bertaud (1970). GRE99 give the classification A3(k) A7(h) F3(m), and note the variability of the RV.

HD 19910. HCK86 gives A2(k) F5(m) according to Drilling & Pesch (1973).

HD 36360. HCK86 gives A5(k) F2(m) according to Slettebak & Nassau (1959), but GRE99 classify the star as A3(k) A7(h) F3(m). Fehrenbach et al. (1987) first put in evidence a variable RV.

HD 102925. Classified as Am by BID88. First discovered as a variable RV star at Mount Wilson Observatory (Wilson & Joy 1950, Abt 1970).

HD 126031. This system is DV Boo (Kazarovets et al. 1999), and was discovered as an eclipsing binary of Algol type by Hipparcos. The period quoted in the Hipparcos catalogue (ESA 1997) is 1.26 days, i.e., exactly the third of the period we found: a stroboscopic effect? (see Sect. 4.4). Classified as Am by BID88 and A3(k) A7(h) F5(m) by GRE99.

HD 127263. An Am star according to BID88, but GRE99 give the classification A2p Sr, and report a variable RV.

HD 138406. Am according to BID88 (but could be a giant: see Sect. 4.2). First reported as a variable RV star by Young (1942) from observations at David Dunlap Observatory.

HD 155714. Visual double ADS 10398 AB = CCDM 17130+0745 AB = STT 325 AB. Δm_{Hp}=1.79; ρ=0.4 arcsec. HCK86 gives A9(k) F1(h) F4(m), according to Abt (1981).

HD 195692. Visual double ADS 13964 AB = CCDM 20320+2548 AB = STF 2695 AB. Δm_{Hp}= 2.17; ρ=0.16 arcsec. Classified A4(k) F0(m) in HCK86, according to Bertaud (1970), and A2(k) F1(h) F0(m) by Abt & Morrell (1995).

HD 199360. HCK86 gives A7(k) F1(h) F5(m), according to Abt (1984), and GRE99 find A5(k) F0(h) F3(m).

Thus, our observations have shown that HD 155714 and HD 195692 are triple systems.

4 PHYSICAL PARAMETERS AND DISCUSSION

4.1 Reddening correction

Strömgren photometry was available for eight objects of our sample (Hauck & Mermilliod 1998). In Table 13, we present the corresponding β, $b-y$, m_1 and c_1 in Cols. 2, 3, 5 and 7. The color excess $E(b-y)$ produced by interstellar reddening (Col. 4) was computed with Crawford (1979)'s calibration of A-type stars. The corresponding indices $(m_1)_0$ and $(c_1)_0$, corrected for reddening, are in Cols. 6 and 8. The index $(\delta m_1)_0 = (m_1)_{\rm std} - (m_1)_0$, where $(m_1)_{\rm std}$ is the standard m_1 corresponding to an A-type star with the same β as the object is given in Col. 9. We used Crawford (1979)'s calibration on the Hyades for determining $(m_1)_{\rm std}$ from β. This index $(\delta m_1)_0$ will be used for the determination of [Fe/H], given in Table 14 (see Sect. 4.2).

For HD 155714, 195692, and 199360, the β indices have not been measured; the values indicated in brackets were obtained from the $(\beta,(b-y)_0)$ relation given by Crawford (1979). We neglected the interstellar absorption for the nearest stars HD 155714 and HD 195692 (with $d < 100$ pc). For HD 199360 ($d = 147$ pc), we used Lucke (1978)'s extinction maps for correcting $b-y$, and then verified that the $E(b-y)$ derived from Crawford (1979), was compatible with Lucke's $E(B-V)$ value. Note that $E(b-y) = 0.73\,E(B-V)$ (Crawford, 1975).

Table 13 shows that the reddening is negligible (i.e., $E(b-y) \leq 0.01$) for HD 36360, 126031, 127263, 155714 and 195692. For HD 19342, 19910 and 199360, we shall use the reddening-corrected values from this table in the following of this paper.

Strömgren photometry was not available for HD 102925 and 138406, which are distant of 114 and 282 pc, respectively (cf. Table 14). The corresponding interstellar extinction values $E(B-V)$, estimated from Lucke (1978)'s galactic charts are 0.03 and 0.06, respectively.

4.2 Physical parameters of the primaries

To estimate some physical parameters of the primaries, which are presented in Table 14, we have used Strömgren photometry and the Hipparcos parallaxes, when those data were available. We have assumed that the photometric contribution of the unseen spectroscopic

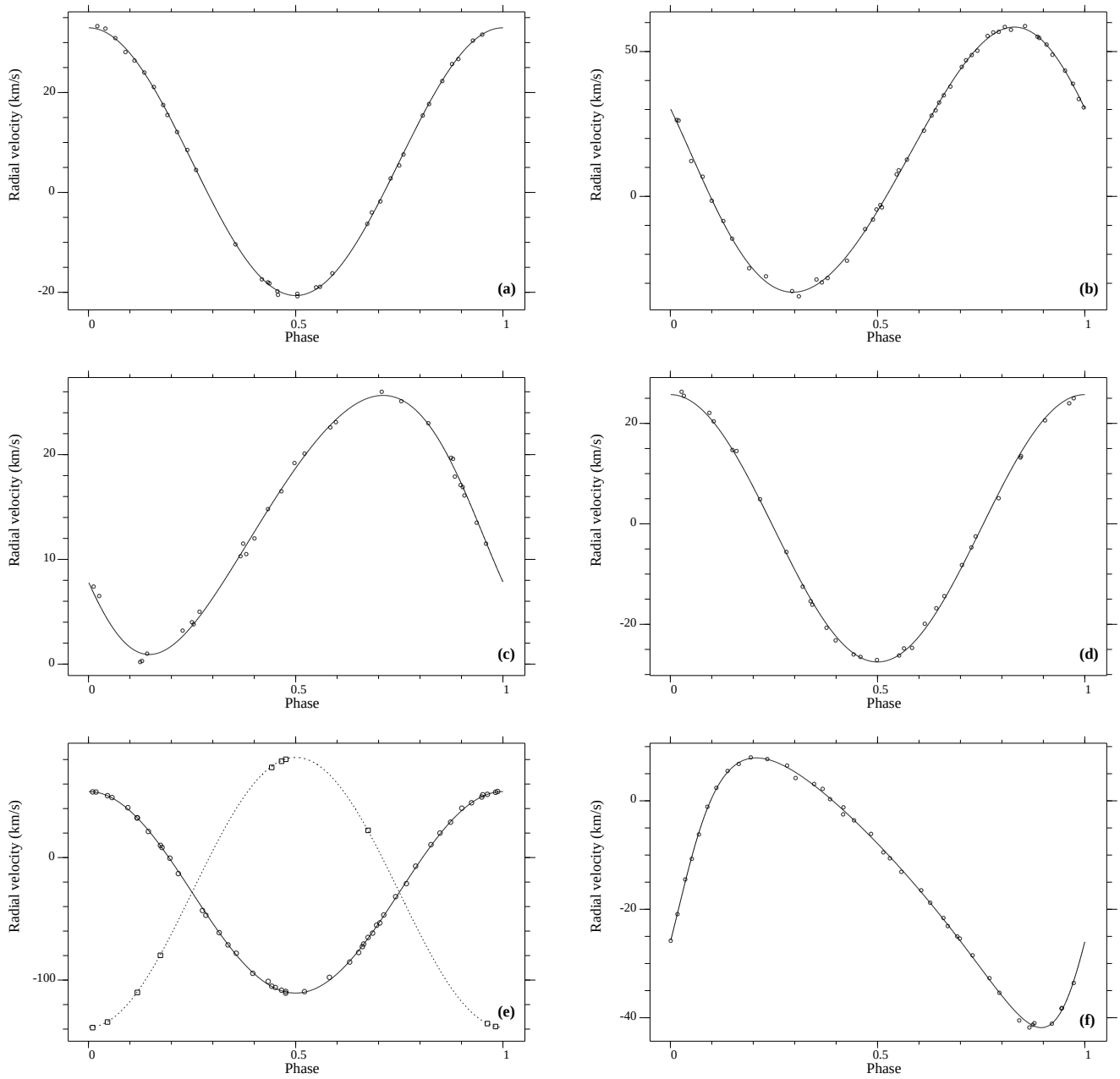

Figure 1. RV curves computed with the orbital elements of Tables 11 and 12: (a) HD 19342, (b) HD 19910, (c) HD 36360, (d) HD 102925, (e) HD 126031, and (f) HD 127263. For HD 19342, HD 102925, and HD 126031 which have circular orbits, the ascending node is taken as the origin of the phases. For the other systems, the origin of the phases corresponds to the periastron passage.

companion was negligible for all systems, except for HD 126031 for which the secondary was detected. We shall discuss the possible influence of the undetected companion in Sect. 4.5. As in Paper V, we proceeded as follows:

1 – From Hipparcos parallaxes π (ESA 1997), we obtained the distances and the visual absolute magnitudes of the systems (except for HD 19910 that was not observed by the satellite), and their errors (Lines 7 and 8).

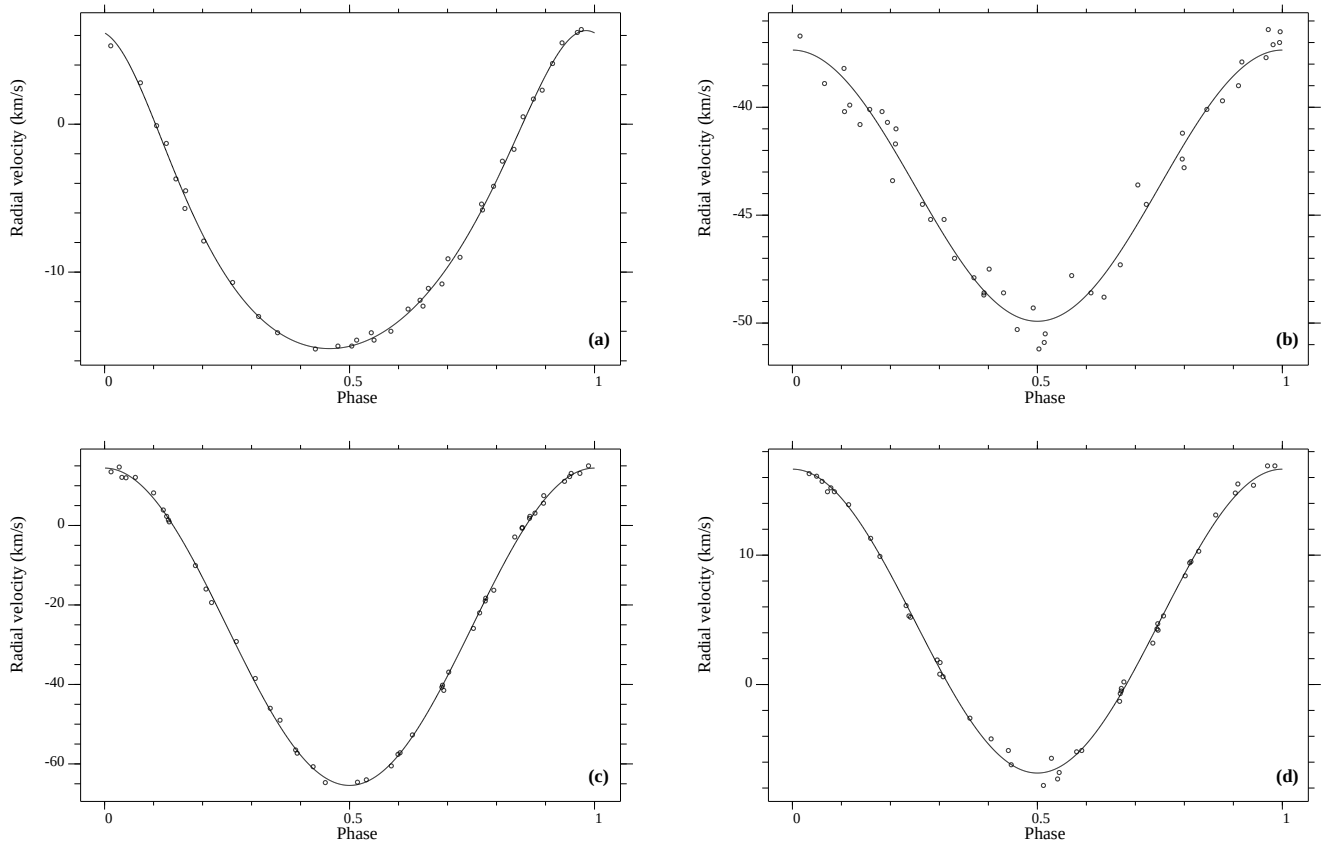

Figure 2. RV curves computed with the orbital elements of Table 11: (a) HD 138406, (b) HD 155714, (c) HD 195692 and (d) HD 199360. For HD 138406, the origin of the phases corresponds to the periastron passage. For the other systems, which have a circular orbit, the ascending node is taken as the origin of the phases.

2 – When Strömgren photometry was available (cf. Sect. 4.1), we deduced the quantities T_{eff} and $\log g$ (Lines 10 and 11) using the $(c_1)_0$ versus β grids of Moon & Dworetsky (1985). For $\log g$ determination, we applied the correction for metallicity proposed by Dworetsky and Moon (1986) for Am stars. The parameter $[Fe/H]$ (line 12) was estimated from the δm_1 versus $[Fe/H]$ correlation, as computed by Cayrel (Crawford, 1975). For HD 102925 and HD 138406, Strömgren photometry was not available: the effective temperature given in Line 10 is based upon the $B-V$ index and Flower (1996)'s calibrations.

3 – The quantities M_V and T_{eff} lead to an estimation of the theoretical radius of the stars (line 13), using the radiation law: $\log(R/\mathrm{R}_\odot) = -0.2M_{bol} - 2\log T_{\mathit{eff}} + 8.47$ (Schmidt-Kaler 1982). The bolometric corrections we used are those tabulated by Flower (1996).

4 – Finally, we report in Fig. 3 the positions of the stars in the theoretical Hertzsprung-Russell diagram, $\log(L/\mathrm{L}_\odot)$ versus $\log T_{\mathit{eff}}$, from Schaller et al (1992), completed with the isochrones computed by Meynet, Mermilliod & Maeder (1993). The positions of the stars in this diagram lead to theoretical estimates of their masses M_1 and ages (Lines 14 and 25 of

Table 1. Radial velocities and $(O-C)$ residuals for HD 19342.

Date (JD) 2400000+	Cycle	RV km.s^{-1}	$(O-C)$ km.s^{-1}
49320.54	-0.07	30.4	0.2
49321.50	-0.05	31.6	-0.1
49324.54	0.02	33.3	0.6
49427.34	2.43	-18.0	0.3
49428.32	2.46	-19.8	-0.2
49432.30	2.55	-19.0	0.4
49640.66	7.44	-18.2	0.4
49643.54	7.50	-20.8	-0.2
49784.32	10.81	15.4	-0.1
49787.33	10.88	25.7	0.3
50123.38	18.76	7.6	-0.3
50127.37	18.85	22.3	-0.1
50323.62	23.46	-20.5	-0.8
50325.61	23.50	-20.3	0.3
50414.47	25.59	-16.2	0.4
50418.52	25.68	-4.0	0.7
50419.41	25.70	-1.8	-0.4
50420.46	25.73	2.8	0.2
50421.35	25.75	5.4	-0.7
50476.39	27.04	32.8	0.7
50477.41	27.06	30.9	0.1
50478.45	27.09	28.1	-0.8
50479.38	27.11	26.4	-0.3
50480.39	27.13	24.0	0.1
50481.37	27.16	21.1	0.3
50482.33	27.18	17.5	0.0
50705.63	32.42	-17.4	-0.2
50738.55	33.19	15.5	-0.4
50739.54	33.21	12.1	-0.1
50740.59	33.24	8.5	0.4
50741.49	33.26	4.5	0.0
50745.54	33.35	-10.4	-0.2
50839.50	35.56	-18.9	0.0
50978.61	38.82	17.7	-0.1
51109.51	41.89	26.7	-0.4
51185.41	43.67	-6.3	0.0

Table 14). Three stars are missing in the diagram: HD 19910, which was not observed by Hipparcos, HD 126031, whose two components are plotted in Fig. 4, and HD 138406 which is not a *classical* Am star and falls beyond its boundaries. Indeed, with the data we have for that star, it could be a hot giant, even though metallic lines are certainly present, as noted by Young (1942) which reported the following comment *"Many very fine lines."* The other stars lie in the main-sequence domain and show different degrees of evolution, the least evolved being HD 127263. The case of the eclipsing binary HD 126031, for which the two components have been detected with ELODIE is dealt with in Sect. 4.4.

Table 2. Radial velocities and $(O-C)$ residuals for HD 19910.

Date (JD) 2400000+	Cycle	RV km.s^{-1}	$(O-C)$ km.s^{-1}
49325.42	0.00	30.7	-0.4
49641.55	20.51	-3.0	0.4
49642.54	20.57	12.7	0.0
49643.46	20.63	27.9	-0.1
49643.61	20.64	29.7	-0.7
49644.58	20.70	44.7	0.2
50125.30	51.89	54.7	0.0
50127.30	52.02	26.2	1.9
50324.64	64.82	57.5	-0.9
50325.62	64.89	55.1	-0.1
50326.65	64.95	43.4	0.1
50327.62	65.02	26.4	0.8
50328.58	65.08	6.8	1.0
50414.45	70.65	32.4	0.0
50415.45	70.71	47.0	0.5
50416.46	70.78	56.6	0.6
50418.45	70.91	52.4	0.1
50419.43	70.97	38.9	0.4
50421.41	71.10	-1.5	-0.5
50476.28	74.66	34.9	-0.2
50477.32	74.73	48.8	-0.2
50478.32	74.79	56.8	-0.3
50479.30	74.86	58.8	1.0
50480.32	74.92	48.9	-0.9
50481.30	74.99	33.6	-1.0
50482.30	75.05	12.2	-2.4
50738.57	91.68	37.9	-0.8
50739.57	91.74	50.3	-0.9
50745.54	92.13	-8.5	0.6
50746.50	92.19	-24.8	-1.4
50838.35	98.15	-14.6	0.0
51106.59	115.55	9.0	1.4
51107.52	115.61	22.7	-0.6
51110.53	115.81	58.5	0.6
52583.49	211.37	-29.7	-0.5^C
52585.52	211.50	-4.5	1.1^C
52600.51	212.47	-11.3	0.5^C
52613.46	213.31	-34.5	-1.6^C
52645.36	215.38	-28.2	-0.6^C
52647.38	215.51	-3.8	-1.3^C
52651.31	215.77	55.4	0.9^C
52660.36	216.35	-28.7	1.8^C
52663.34	216.55	7.6	1.3^C
52689.31	218.23	-27.6	1.9^C
52690.28	218.29	-32.7	0.4^C
52692.32	218.43	-22.2	-1.7^C
52693.29	218.49	-8.0	-0.4^C

4.3 Masses and separations of the secondaries

From the values computed for $f(m)$ and $a_1 \sin i$ (Table 11), and assuming for the primaries the theoretical masses M_1 (Table 14), we can obtain, for a given value of the orbital inclination i, the values of M_2, the mass of the secondary, and a, the true mean separation of the components. For that, we use the formulae:

$$f(m) = M_1 \times \sin^3 i \times \mu^3 \,/\, (1+\mu)^2, \qquad (1)$$

Table 3. Radial velocities and $(O-C)$ residuals for HD 36360.

Date (JD) 2400000+	Cycle	RV km.s^{-1}	$(O-C)$ km.s^{-1}
48939.51	-0.88	0.2	-0.9
48940.49	-0.87	0.3	-0.7
48966.57	-0.75	4.0	0.4
48967.46	-0.75	3.8	0.0
48970.53	-0.73	5.0	0.5
49318.50	0.87	19.7	0.4
49319.54	0.88	19.6	0.7
49320.46	0.88	17.9	-0.7
49323.48	0.90	17.1	-0.3
49324.56	0.90	16.9	0.0
49325.49	0.91	16.1	-0.5
49426.39	1.37	11.5	0.6
49432.31	1.40	12.0	-0.6
49641.57	2.37	10.3	-0.2
49644.57	2.38	10.5	-0.9
49715.36	2.71	26.0	0.3
49725.57	2.75	25.1	-0.1
49781.37	3.01	7.4	0.6
49784.27	3.03	6.5	0.8
50124.49	4.60	23.1	-0.2
50324.65	5.52	20.1	0.2
50414.59	5.94	13.5	-0.3
50419.47	5.96	11.5	-0.1
50477.47	6.23	3.2	0.5
50738.61	7.43	14.8	0.1
50745.62	7.47	16.5	-0.2
50822.42	7.82	23.0	0.1
51108.56	9.14	1.0	0.1
51185.56	9.50	19.2	0.6
52936.63	17.58	22.6	-0.2

where $\mu = M_2/M_1$ is the mass-ratio in the system, and

$$a = a_1 + a_2 = (a_1 \sin i) \times (1 + 1/\mu)/\sin i. \qquad (2)$$

The minimum values for μ, M_2 and a correspond to $\sin i = 1$ (i.e., $i = 90°$). As for the maxima of those quantities, they can be approximated taking into account the absence of CORAVEL correlation dips from the secondary spectroscopic components, that implies roughly $\Delta m_V \geq 2.0$, i.e., via the mass–luminosity relation, $\mu \leq 0.6$. Following that procedure, we give in Table 14: (i) on one hand M_{2min} and a_{min}, the minimum values that we found when $i = 90°$ for M_2 and a, respectively (Lines 15 and 17), (ii) on the other hand M_{2max} and a_{max}, the maximum values of M_2 and a (Lines 16 and 18), obtained with the minimum value of i corresponding to $\mu = 0.6$ (Line 21). For HD 19910, for which no theoretical value could be derived, we assumed $M_1 = 2$ M$_\odot$, a typical value for A-type stars. Notice that, as already pointed out by Carquillat et al. (1982), the separation we obtain with (2) has a very small dependence on the value of i, and we can conclude that all those binary systems are detached.

Table 4. Radial velocities and $(O-C)$ residuals for HD 102925.

Date (JD) 2400000+	Cycle	RV km.s^{-1}	$(O-C)$ km.s^{-1}
49787.57	-0.66	-15.4	-0.5
50124.63	19.84	13.2	-0.8
50125.61	19.90	20.6	-0.4
50126.57	19.96	24.0	-1.0
50127.63	20.03	26.3	1.0
50192.49	23.97	25.0	-0.4
50193.47	24.03	25.5	0.3
50194.48	24.09	22.1	0.9
50195.39	24.15	14.7	-0.1
50415.69	37.55	-26.2	-0.1
50416.71	37.61	-19.9	1.1
50418.72	37.74	-2.5	0.6
50419.64	37.79	5.1	-1.0
50477.61	41.32	-12.5	-0.4
50478.56	41.38	-20.7	-0.8
50479.63	41.44	-26.0	-0.2
50480.56	41.50	-27.1	0.4
50481.63	41.56	-24.8	0.6
50609.49	49.34	-16.1	-0.6
50610.42	49.40	-23.2	-0.9
50611.40	49.46	-26.5	0.1
50613.45	49.58	-24.7	-0.8
50614.41	49.64	-16.8	0.8
50615.43	49.70	-8.2	0.3
50835.70	63.10	20.4	0.2
50836.61	63.16	14.5	1.1
50837.54	63.22	4.9	0.2
50838.59	63.28	-5.6	0.3
50976.35	71.66	-14.4	0.6
50977.42	71.73	-4.7	0.1
50979.39	71.85	13.5	-0.7

The two short-period systems HD 155714 and HD 199360 have very low mass functions, that permit a wide range of possibilities for i, the orbital inclination, and M_2, the mass of the companion. As an indication, the (very plausible) hypothesis of rotation–revolution synchronism (see Sect 4.7) would imply $i = 33°$, $M_2 = 0.1\mathrm{M}_\odot$ for HD 155714 and $i = 14°$, $M_2 = 0.5\mathrm{M}_\odot$ for HD 199360. Such masses are those of red dwarf stars.

4.4 The eclipsing binary HD 126031

The light curve of HD 126031 provided by Hipparcos is plotted in phase in Fig. 5, using the period of 3.78 days found with our spectroscopic observations. It clearly shows two eclipses with two peaked minima. The period quoted in the Hipparcos catalogue (1.26 days) is definitely false and must be due to a stroboscopic effect.

We performed an analysis of that curve using two programs: EBOP, from Popper & Etzel (1981) that fits the light curve only, and WD (version 1996), from Wilson & Devinney (1971) that performs a fit which also takes into account the radial velocity orbital parameters. Note

Table 5. Radial velocities and $(O-C)$ residuals for HD 126031.

Date (JD) 2400000+	Cycle	RV_1 km.s^{-1}	$(O-C)_1$ km.s^{-1}	RV_2 km.s^{-1}	$(O-C)_2$ km.s^{-1}
50479.75	-0.15	20.0	0.8	–	–
50480.69	0.09	40.7	1.1	–	–
50611.45	34.66	-70.6	0.1	–	–
50614.43	35.45	-106.1	0.6	–	–
50615.38	35.70	-53.4	-1.1	–	–
50615.52	35.74	-31.9	1.1	–	–
50834.74	93.70	-55.2	0.9	–	–
50835.71	93.95	51.2	1.2	–	–
50836.71	94.22	-13.1	-1.8	–	–
50837.70	94.48	-110.7	-1.0	–	–
50839.63	94.99	53.9	0.3	–	–
50839.75	95.02	53.5	0.2	–	–
50974.45	130.63	-85.3	-0.7	–	–
50974.54	130.65	-77.5	-1.6	–	–
50975.48	130.90	40.3	1.9	–	–
50976.40	131.14	21.3	-0.9	–	–
50976.52	131.18	8.2	0.4	–	–
50977.35	131.40	-94.5	-0.7	–	–
50977.49	131.43	-101.1	2.5	–	–
50978.35	131.66	-72.7	-0.6	–	–
50978.45	131.69	-61.7	-1.0	–	–
50978.55	131.71	-46.9	0.7	–	–
50979.35	131.92	44.7	0.0	–	–
50979.44	131.95	49.4	-0.3	–	–
51931.62	383.67	-65.2	0.7	22.2	0.4^E
52039.43	412.17	9.9	0.3	-79.8	-0.6^E
52040.53	412.47	-108.3	0.4	78.6	-0.6^E
52040.57	412.48	-109.3	0.4	80.2	-0.3^E
52042.41	412.96	51.6	0.0	-135.5	-0.1^E
52042.59	413.01	53.6	-0.1	-138.8	-0.5^E
52297.66	480.44	-105.0	0.2	73.6	-0.9^E
52299.70	480.98	53.3	0.0	-137.9	-0.1^E
52303.73	482.05	50.5	0.0	-134.2	-0.3^E
52489.35	531.12	32.4	0.1	-110.1	-0.5^E
52721.61	592.52	-109.4	0.5^C	–	–
52730.51	594.87	28.9	-0.4^C	–	–
52747.47	599.36	-78.1	1.3^C	–	–
52758.54	602.28	-47.1	-1.7^C	–	–
52760.59	602.83	10.5	0.9^C	–	–
52765.48	604.12	32.4	-0.1^C	–	–
52769.56	605.20	-0.5	0.7^C	–	–
52775.50	606.77	-21.3	-1.8^C	–	–
52777.57	607.32	-61.3	0.0^C	–	–
52811.46	616.28	-43.2	-1.9^C	–	–
52814.42	617.06	49.0	0.3^C	–	–
52815.48	617.34	-71.3	-0.3^C	–	–
52816.41	617.58	-97.8	2.3^C	–	–
52866.37	630.79	-7.0	1.2^C	–	–

that the results should be considered as preliminary, since the residuals are rather large and the light curve is under-sampled, especially around the minima.

The parameters found by WD and EBOP are in very good agreement; the mean values are displayed in Table 15. The fitted solution and the residuals are plotted in Fig. 5. The two solutions have an rms error smaller than 0.01 mag., and do not show any difference in that plot.

Table 6. Radial velocities and $(O-C)$ residuals for HD 127263.

Date (JD) 2400000+	Cycle	RV km.s^{-1}	$(O-C)$ km.s^{-1}
50480.72	-0.52	-6.1	0.6
50609.51	8.53	-10.6	-0.3
50611.50	8.67	-23.1	-0.2
50614.48	8.88	-41.0	0.6
50615.41	8.94	-38.3	0.5
50834.72	24.35	3.1	0.3
50835.72	24.42	-2.5	-0.8
50837.72	24.56	-13.1	-0.5
50839.64	24.69	-25.0	0.1
50974.52	34.17	6.8	-0.2
50975.50	34.23	7.7	0.0
50976.47	34.30	4.2	-1.0
50977.40	34.37	2.2	0.6
50978.48	34.44	-3.6	0.0
50979.48	34.51	-9.5	-0.5
51106.26	43.42	-1.2	0.5
51109.24	43.63	-18.8	0.0
51110.26	43.70	-25.4	0.3
51185.75	49.00	-25.8	-0.1
51186.72	49.07	-6.2	-0.4
52691.73	154.77	-32.7	0.3^C
52721.58	156.87	-41.8	-0.7^C
52736.59	157.92	-41.1	0.0^C
52751.58	158.97	-33.6	-0.4^C
52753.54	159.11	2.4	0.2^C
52760.58	159.61	-16.5	0.3^C
52766.44	160.02	-20.9	-0.2^C
52767.47	160.09	-1.1	0.3^C
52775.58	160.66	-21.6	0.2^C
52777.50	160.79	-35.4	0.0^C
52795.41	162.05	-10.7	-0.4^C
52809.42	163.04	-14.5	0.5^C
52821.36	163.87	-41.3	0.1
52822.37	163.95	-38.2	0.4
52833.53	164.73	-28.5	0.3^C
52841.40	165.28	6.5	0.3^C
52854.39	166.19	8.0	0.2^C
52871.35	167.39	0.3	-0.1^C
52896.31	169.14	5.5	0.2^C
52906.33	169.84	-40.5	-0.9^C

The two models WD and EBOP lead to $\Delta m_{Hp} = 1.38 \pm 0.08$, and $\Delta m_{Hp} = 1.28 \pm 0.08$, respectively. Given the closeness of the effective temperatures of the two components, $\Delta m_{Hp} \approx \Delta m_V$ (the corresponding differential correction is negligible: $\sim$0.02 mag.). Hence the analysis of the light curve leads to $\Delta m_V = 1.33 \pm 0.1$ We also obtained an independent estimate of $\Delta m_V \sim 1.57 \pm 0.2$ from the ELODIE correlation dips of the two components, using the relation $\Delta m_V = -2.5 \log[(S_1/S_2) \times (T_{eff2}/T_{eff1})]$, where S_1 (resp. S_2) is the surface of the correlation dip of component 1 (resp. 2) (Duquennoy, 1994, private communication). Hence we finally adopted the weighted mean value of the two determinations, from the light curve and ELODIE, i.e., $\Delta m_V = 1.41 \pm 0.15$.

Table 7. Radial velocities and $(O-C)$ residuals for HD 138406.

Date (JD) 2400000+	Cycle	RV km.s^{-1}	$(O-C)$ km.s^{-1}
49786.64	-0.23	-5.8	-0.1
49787.69	-0.19	-2.5	0.5
50127.71	12.96	6.2	0.0
50192.63	15.48	-15.0	0.1
50193.62	15.51	-14.6	0.3
50194.54	15.55	-14.6	-0.2
50326.38	20.65	-12.3	-0.5
50327.38	20.69	-10.8	-0.6
50328.33	20.73	-9.0	-0.6
50329.46	20.77	-5.4	0.4
50415.72	24.11	-0.1	0.1
50416.74	24.15	-3.7	-0.3
50419.73	24.26	-10.7	0.2
50477.72	26.50	-15.0	0.0
50478.75	26.54	-14.1	0.4
50480.70	26.62	-12.5	0.3
50610.58	31.64	-11.9	0.1
50614.46	31.79	-4.2	0.0
50615.54	31.84	-1.7	-0.4
50738.30	36.58	-14.0	-0.3
50740.28	36.66	-11.1	0.2
50741.31	36.70	-9.1	0.5
50745.28	36.85	0.5	0.4
50746.29	36.89	2.3	-0.6
50834.73	40.31	-13.0	0.0
50835.73	40.35	-14.1	-0.1
50837.72	40.43	-15.2	-0.1
50978.48	45.88	1.7	0.1
50979.49	45.91	4.1	-0.1
51009.45	47.07	2.8	0.3
51109.25	50.93	5.5	0.3
51110.27	50.97	6.4	0.1
51111.29	51.01	5.3	-0.6
52820.41	117.13	-1.3	0.5
52821.39	117.16	-5.7	-0.8
52821.43	117.17	-4.5	0.5
52822.38	117.20	-7.9	-0.3

From the knowledge of the ratio T_{eff1}/T_{eff2} (Line 4 of Table 15), the global $B-V$ index (Line 4 of Table 14) and this determination of Δm_V, we computed the correction ΔT to be applied to T_{eff1} as determined by Strömgren photometry, due to the presence of the companion. This was done with an iterative process, which used Flower (1996)'s table of T_{eff} versus $B-V$ for main sequence stars. We obtained: $T_{eff1} = 7370 \pm 80$ K, $T_{eff2} = 6410 \pm 80$ K, $(B-V)_1 = 0.31 \pm 0.02$ and $(B-V)_2 = 0.47 \pm 0.02$.

From the global value $M_V = 1.88$, as determined with Hipparcos parallax, and $\Delta m_V = 1.41 \pm 0.15$, we obtain $M_{V1} = 2.14 \pm 0.3$ and $M_{V2} = 3.54 \pm 0.3$. When applying the bolometric corrections $BC_1 = 0.03$ and $BC_2 = -0.02$, corresponding to the component temperatures T_{eff1} and T_{eff2} (Flower, 1996), we find $\log(L_1/L_\odot) = 1.03 \pm 0.15$ and $\log(L_2/L_\odot) = 0.49 \pm 0.15$. Both components of HD 126031 are plotted in Fig. 4. Their location on this theoretical

Table 8. Radial velocities and $(O-C)$ residuals for HD 155714.

Date (JD) 2400000+	Cycle	RV km.s^{-1}	$(O-C)$ km.s^{-1}
46963.71	-653.86	-40.8	-1.2^N
47370.70	-531.82	-40.2	0.9^N
47995.82	-344.36	-48.8	-1.0^N
48350.91	-237.88	-39.9	-0.9^N
49141.50	-0.81	-40.7	0.8
49142.50	-0.51	-49.3	0.6
49143.51	-0.20	-41.2	0.6
49144.54	0.11	-38.2	0.5
49145.50	0.39	-48.6	-0.1
49145.63	0.43	-48.6	0.7
49146.54	0.71	-43.6	1.8
49147.51	1.00	-36.5	0.9
49427.70	85.02	-36.7	0.7
49428.68	85.31	-45.2	0.7
49429.68	85.61	-48.6	-0.1
49430.68	85.91	-39.0	-0.7
49431.68	86.21	-41.7	0.4
49432.66	86.50	-51.2	-1.3
49787.71	192.97	-36.4	1.1
50192.61	314.39	-48.7	-0.2
50194.58	314.98	-37.1	0.3
50195.59	315.28	-45.2	-0.3
50325.38	354.20	-43.4	-1.5
50326.42	354.52	-50.5	-0.6
50327.37	354.80	-42.8	-1.1
50328.39	355.11	-40.2	-1.5
50329.38	355.40	-47.5	1.3
50480.75	400.80	-42.4	-0.5
50611.47	439.99	-37.0	0.4
50614.55	440.92	-37.9	0.3
50615.53	441.21	-41.0	1.1
50739.32	478.33	-47.0	-0.3
50743.26	479.51	-50.9	-1.0
50837.74	507.85	-40.1	0.0
50974.57	548.88	-39.7	-0.6
50975.51	549.16	-40.1	0.1
50976.51	549.46	-50.3	-0.6
50977.39	549.72	-44.5	0.2
50978.54	550.07	-38.9	-1.0
51106.27	588.37	-47.9	0.0
51107.27	588.67	-47.3	-0.6
51108.26	588.97	-37.7	-0.2
51109.26	589.27	-44.5	-0.3
51110.27	589.57	-47.8	1.5

diagram is in good agreement with the mass determination from the light curve (Table 15), and they are located on the same isochrone of $\sim 10^9$ years, within the error bars.
Hence all parameters that we found for the secondary (radius, temperature, mass and luminosity) are consistent and suggest a late F dwarf star (F6/7 V).

Table 9. Radial velocities and $(O-C)$ residuals for HD 195692.

Date (JD) 2400000+	Cycle	RV km.s^{-1}	$(O-C)$ km.s^{-1}
47459.39	-60.10	5.6	-0.6
48133.42	-0.41	-60.5	-0.7
48135.45	-0.23	-22.0	-0.4
48136.44	-0.15	-0.5	1.0
48137.41	-0.06	11.1	-0.4
48936.35	70.69	-40.2	0.1
48937.34	70.78	-18.3	0.2
48939.28	70.95	12.3	-0.1
48940.25	71.04	12.1	-1.4
48941.28	71.13	2.3	-0.2
48966.25	73.34	-46.0	0.5
48967.24	73.43	-60.7	0.4
48969.25	73.60	-57.2	0.1
48970.25	73.69	-41.5	-1.9
48972.24	73.87	2.3	0.8
49141.61	88.87	1.8	0.5
49143.61	89.04	12.0	-0.9
49144.58	89.13	1.4	-0.4
49145.58	89.22	-19.4	-1.8
49146.59	89.31	-38.5	1.1
49147.55	89.39	-57.3	-0.6
49318.32	104.52	-64.6	0.6
49319.26	104.60	-57.6	0.4
49320.27	104.69	-40.7	-0.1
49321.27	104.78	-19.0	-0.2
49323.25	104.95	13.1	0.4
49325.28	105.13	0.9	-0.6
49644.38	133.39	-56.5	-0.3
50191.62	181.85	-0.7	0.9
50193.63	182.03	14.7	1.0
50194.64	182.12	3.9	0.3
50195.63	182.21	-16.0	-1.2
50323.54	193.53	-64.0	0.5
50325.44	193.70	-36.9	0.4
50326.48	193.79	-16.3	-1.8
50327.43	193.88	3.1	-0.3
50328.46	193.97	13.1	-0.6
50329.51	194.06	12.1	0.7
50419.29	202.01	13.5	-0.8
50420.27	202.10	8.2	1.4
50421.23	202.19	-10.1	-0.4
50738.36	230.27	-29.2	1.0
50740.41	230.45	-64.7	-1.2
50745.44	230.90	7.5	1.2
50746.47	230.99	15.0	0.7
50976.50	251.36	-49.0	1.6
50979.55	251.63	-52.7	0.4
52821.59	414.75	-25.9	-1.1
52822.55	414.84	-2.9	1.8

4.5 Influence of the undetected companions

As already mentioned, we assumed that the photometric contribution of the companion was negligible for the other systems which were detected as SB1 only. The absence of a secondary correlation dip in the VR data, implies a large magnitude difference between the two components (roughly $\Delta m_V \geq 2.0$) or a large spin velocity for the companion ($v \sin i >$

Table 10. Radial velocities and $(O-C)$ residuals for HD 199360.

Date (JD) 2400000+	Cycle	RV km.s^{-1}	$(O-C)$ km.s^{-1}
49642.36	0.81	9.4	0.1
49643.34	1.30	1.7	0.5
49644.34	1.80	8.4	-0.3
50324.46	342.09	14.9	-0.1
50325.45	342.58	-5.2	0.2
50326.45	343.08	15.2	0.0
50327.32	343.51	-7.8	-1.0
50327.47	343.59	-5.1	-0.1
50327.64	343.68	0.2	0.5
50328.36	344.03	16.3	-0.1
50329.35	344.53	-5.7	1.0
50329.63	344.67	-0.3	0.4
50416.33	388.05	16.1	0.0
50418.38	389.07	14.9	-0.6
50419.32	389.54	-6.8	-0.4
50420.35	390.06	15.7	-0.1
50421.31	390.54	-7.3	-0.9
50609.62	484.76	5.3	-0.1
50611.60	485.75	4.2	-0.4
50615.59	487.75	4.7	0.1
50738.38	549.18	9.9	-0.1
50738.50	549.24	5.2	-0.4
50739.36	549.67	-0.7	0.1
50740.34	550.16	11.3	0.1
50740.50	550.24	5.3	-0.5
50741.36	550.67	-1.3	-0.4
50741.51	550.74	4.3	-0.2
50745.36	552.67	-0.5	0.2
50745.49	552.74	3.2	-0.6
50746.25	553.11	13.9	0.2
50746.48	553.23	6.1	-0.1
50975.59	667.86	13.1	0.5
50976.48	668.31	0.6	-0.1
50976.59	668.36	-2.6	0.1
50977.52	668.83	10.3	-0.2
51106.37	733.30	1.9	0.3
51107.41	733.81	9.5	0.0
51110.38	735.30	0.8	-0.4
52820.47	1590.91	15.5	0.7
52820.59	1590.97	16.9	0.5
52821.46	1591.41	-4.2	0.6
52821.54	1591.44	-5.1	0.9
52821.55	1591.45	-6.2	0.0
52822.46	1591.90	14.8	0.2
52822.54	1591.94	15.4	-0.4
52824.62	1592.98	16.9	0.3

40 km.s^{-1}). As we shall see in Sect. 4.7, tidal interaction between the two stars tend to reduce the spin velocity which makes the latter possibility rather unlikely. Another possibility for accounting for the absence of detection of the secondary could be that the companion is a hot star without metallic lines (e.g, A-type star). But the values of the mass function that we found ($f(m) \leq 0.15$ M$_\odot$) for those objects implies that, statistically, the companion has a mass of $M_2 \leq 1.4$ M$_\odot$ (value obtained with $i = 60°$ and $M_1 = 2$ M$_\odot$), which corresponds to a star of F5-type or later. Note that the spectrum of such stars exhibits metallic lines which

make those stars detectable by CORAVEL when $\Delta m_V < 2$. Hence the absence of detection suggests that the companions are not brighter than this limit.

In the case of a companion with $\Delta m_V \sim 2$, the locations of the primaries in the HR diagram of Fig 3 would be slightly shifted to the bottom left (about -0.06 in $\log L$ and $+0.006$ in $\log T$), since their luminosities would be overestimated and their temperatures underestimated.

4.6 Circularization of the orbits

4.6.1 Zahn's theory of dynamical tides

Dissipative phenomena occurring in tidal interaction between components of close binaries lead to orbital circularization and synchronization between spin and orbital period. For stars with an outer radiative zone, like Am stars, Zahn (1975, 1977) proposed that the main dissipative mechanism was radiative damping acting on the *"dynamical tide"*. In that case, Zahn showed that the circularization timescale, t_{circ} (defined such that $1/t_{circ} = -\dot{e}/e$), is a steep function of the fractional radius R/a:

$$\frac{1}{t_{circ}} = \frac{21}{2}\left(\frac{GM}{R^3}\right)^{1/2} q\,(1+q)^{11/6}\,E_2\,\left(\frac{R}{a}\right)^{21/2} \qquad (3)$$

where E_2 is related with the dynamic tidal contribution to the total perturbed potential. The tidal constant E_2 is dependent on the stellar structure and strongly varies with mass and time:

- For a given mass, it is a strongly decreasing function of the convective core size. Thus, when the star evolves off the main sequence, its core shrinks and E_2 decreases very quickly. E_2 can change in several decades during stellar evolution for a given mass (Claret & Cunha, 1997).
- For nearly homogeneous models of stars near the ZAMS, with masses of 1.6 to 5 $M_\odot$, $\log E_2$ changes from -8.5 to -6.8 (Zahn, 1975, and Claret & Cunha, 1997).

The strong dependence of E_2 on the internal stellar structure, which is unfortunately badly known, induces large uncertainties on t_{circ}.

To compute t_{circ} for our systems (Line 26 of Table 14) we performed a parabolic interpolation of the tabulated E_2 values computed by Zahn (1975), which are in very good agreement with more recent computations by Claret & Cunha (1997). Except for HD 126031, for which q was known, we assumed $q = 0.5$ for all systems (note that t_{circ} has a small dependence on

q). In all cases, the characteristic circularization times we found are larger (for HD 199360), or much larger (for the other systems) than the ages of the stars. Hence the circular orbits of HD 19342, 102925, 126031, 155714, 195692 and 199360 cannot be explained by tidal effects acting on the Am stars during their life in the main sequence, in the context of Zahn's theory (see discussion in next section).

4.6.2 Curve of e versus R/a

In Eq. 3 we have seen that Zahn's theory stressed the importance of the "fractional radius" parameter (R/a), and predicted that $t_{circ} \propto (R/a)^{-21/2}$. Indeed, Giuricin et al. (1984) showed on a sample of 200 early-type binaries (O, B, A-type) that the transition between eccentric and circular, or quasi-circular (i.e., $e < 0.05$) orbits was rather sharp and occurred at about $(R/a)_c \sim 0.24$, which agreed well with Zahn's theory.

Following those authors, we computed the fractional radius for each object of our sample (Line 20 of Table 14), by using for a the mean value $\overline{a}$ of a_{min} and a_{max} (Line 19). The resulting plot (Fig 6) suggests that the critical value of the fractional radius is $(R/a)_c \sim 0.15$. This is smaller than that proposed by Giuricin et al., that was in full agreement with Zahn's model. Hence this plot illustrates also the discrepancy that we find with Zahn's predictions: there are more circularized systems than what is expected from models with radiative dissipation of dynamical tides.

However, let us recall that Eq. 3 is valid for homogeneous systems, made of two stars possessing a radiative envelope. As seen in Sect. 4.5, our systems are not homogeneous, and the unseen companions are likely to be convective late-type stars, with masses less than 1.4 $M_\odot$. For stars having a convective envelope, dissipation by turbulent viscosity is the dominant process. According to Zahn & Bouchet (1989), the circularization of orbits takes place in the very beginning of the Hayashi phase of pre-main sequence phase, for late-type binaries. There is little further decrease of the eccentricity on the main sequence. Hence the convective dissipation acting on the cool companion may circularize the orbit of a non-homogeneous binary system. Zahn & Bouchet showed that the theoretical cut-off period, which separates the circular from the eccentric systems is $P \sim 8$ days for convective stars with masses ranging from 0.5 to 1.25 $M_\odot$. This would provide a natural explanation for the presence of circular orbits for the shortest period systems of our sample, namely HD 126031,

155714 and 199360. The case of HD 19342 and 102925 with periods longer than 42 days and 16 days, respectively, is more puzzling: those systems may have formed as circular, indeed.

4.7 Rotation–revolution synchronism

In Paper V, we studied eight binaries with orbital period $P \leq 10$ days, and concluded that all those systems have probably reached the rotation–revolution synchronism state. In the present sample, as seven out of ten binaries had periods larger than 10 days, it was interesting to test the rotation–revolution synchronism for those objects.

4.7.1 Kitamura & Kondo's test

For that purpose, we used a test which consists in comparing the radius R_1 of the primary with R_{sync}, the expected value of the radius obtained when assuming that (i) synchronism has been reached, and (ii) that the orbit and the equator of the star are coplanar. In that case we have the relation:

$$R_{sync} = \frac{v\,P}{50.6} = \frac{v \sin i\; P}{50.6 \sin i} \tag{4}$$

where v is the tangential equatorial velocity in km.s^{-1}, P is the orbital period in days, and R_{sync} is the star radius in solar radii. The quantity $v \sin i$ is an observational datum, that can be derived from the analysis of the CORAVEL correlation dips (see Benz & Mayor 1981, 1984). The value of $v \sin i$ for each star of the sample was calculated by S. Udry at Geneva Observatory and is given in Line 5 of Table 14. Unfortunately, i is unknown for all the systems we studied, except for HD 126031 which presents eclipses. Nevertheless, as $\sin i \leq 1$, the relation (4) implies:

$$R_1 \geq R_{sync,min} \qquad \text{with} \quad \mathrm{R}_{sync,\,min} = \mathrm{v \sin i \times P/50.6} \tag{5}$$

which is a necessary condition for synchronism, and known as Kitamura and Kondo (1978)'s test (hereafter KK-test). Indeed, given P and $v \sin i$, a star with a radius R_1, such that $R_1 < R_{sync}$, has an angular rotation which is too large for synchronism. The values of $R_{sync,\,min}$ are given in Line 22 of Table 14 Notice that for the eccentric orbits, namely for HD 36360, 127263 and 138406, we must take into account the pseudo-synchronous rotation period (see Hut 1981, formulae 44 and 45) instead of the orbital period, i.e., 201.5, 8.7 and 20.3 days, respectively.

Comparing those values to the theoretical values of the radii (Line 13 of Table 14), we see that the last six stars of the list (HD 126031 to HD 199360) satisfy the inequality (5), taking into account the quoted errors: therefore they are likely to rotate in synchronism or pseudo-synchronism (in Line 23, we put "likely" synchronism for those objects). As expected, among the synchronized stars we find the systems with the shortest periods, namely HD 126031, 155714 and 199360.

4.7.2 Comparison with Zahn's theory

With the same theoretical description of radiative dissipation induced by tidal effects that we described in Sect. 4.6, Zahn (1975) also predicted values for t_{sync}, the characteristic synchronization time of binary systems. He obtained:

$$\frac{1}{t_{sync}} = 5 \times 2^{5/3} \times \left(\frac{GM}{R^3}\right)^{1/2} q^2 \, (1+q)^{5/6} \, E_2 \, \frac{MR^2}{I} \, \left(\frac{R}{a}\right)^{17/2} \tag{6}$$

where I is the momentum of inertia of the star.

Like for t_{circ} (Sect. 4.6), we computed the values of t_{sync} using the tabulated E_2 and MR^2/I of Zahn (1975), with $q = 0.5$ for all systems, except for HD 126031 for which $q = 0.75$ was known. The corresponding values are displayed in Line 27 of Table 14.

Here, the agreement with Zahn's radiative theory is better than for t_{circ} (see Sect. 4.6):

- all systems for which KK-test is negative have $t_{sync} \gg t_{age}$, where t_{age} is the age of the star (Line 25 of Table 14);
- for HD 199360, $t_{sync} \ll t_{age}$ and indeed this system is very likely to be synchronized (since KK-test is positive and the period is very short, $P = 1.99$ d);
- the agreement with Zahn's theory is marginal with $\log t_{sync} \sim \log t_{age}$ for HD 126031 (synchronized) and HD 155714 (very likely to be synchronized with a positive KK-test and a very short period).

The only clear possible disagreement is found for the systems HD 127263, 138406 and 195692 which have a positive KK-test and $t_{sync} > t_{age} \times 10^2$.

Hence the tidal effects seem more efficient for synchronizing binaries than what is expected from Zahn's theory of radiative dissipation. A possible explanation could be that synchronization by tidal effects starts from the upper layers of the star and then proceeds inwards to the center (J.-P. Zahn, 2003, private communication). As observational data (rotation velocity) concern the surface of the star, there is a possible bias of considering as synchro-

nized stars objects for which synchronism state is not fully reached on the whole star. A theoretical problem would then be to derive the characteristic time t_{start} when the process starts in the surface and the typical duration Δt_{mig} of this migration process, from the surface to the center. For HD 127263, 138406 and 195692, this time would be very large with $t_{start} \leq 10^{-2}\, t_{sync}$ and $\Delta t_{mig} \sim t_{sync}$.

As a general conclusion of this section and Sect. 4.6, the radiative dissipation of dynamical tides as presented by Zahn (1975) is not efficient enough to circularize and synchronize the binary systems we have studied. Two possibilities may partially account for this situation:

- Circularization of the orbit is performed with a greater efficiency by convective dissipation of tidal effects acting on the cool companion during the pre-main sequence stage.
- Synchronization of the radiative primaries is suggested by observations much earlier than the characteristic times indicate, since the process starts from the surface.

Acknowledgments: This work is based on observations made at the Haute-Provence Observatory (France) and at Cambridge Observatory (U.K.).
We are grateful to R. Griffin for observing to our request some stars of our observing programme. We are indebted to M. Mayor, Director of Geneva Observatory, for giving us observing time with CORAVEL, and to S. Udry for reducing our observations in the RV Geneva data base. We thank J.-L. Halbwachs and M. Imbert for making two observations of HD 36360 at OHP. We are also grateful to J.-P. Zahn for fruitful discussions about the theoretical aspects of tidal dissipation.
For bibliographic references, we used the SIMBAD data base, operated by the "Centre de Données Astronomiques de Strasbourg" (France).

REFERENCES

Abt H.A., 1970, ApJS, 19, 387

Abt H.A., 1981, ApJS, 45, 437

Abt H.A., 1984, ApJ, 285, 247

Abt H.A., Morrell N.I., 1995, ApJS, 99, 135

Baranne A., Mayor M., & Poncet J.L., 1979, Vistas Astron., 23, 279

Baranne A., Queloz D., Mayor M., Adrianzyk G., Knispel G., Kohler D., Lacroix D., Meunier J.-P., Rimbaud G., Vin A., 1996, A&AS, 119, 373

Benz W., Mayor M., 1981, A&A, 93, 235

Benz W., Mayor M., 1984, A&A, 138, 183

Bertaud C., 1970, A&AS, 1, 7

Bidelman W.P., 1988, PASP, 100, 1084

Carquillat J.-M., Nadal R., Ginestet N., Pédoussaut, A., 1982, A&A, 115, 23

Carquillat J.-M., Ginestet N., Prieur J.-L., Debernardi J.-Y., 2003, MNRAS, 346, 555.

Claret A., Cunha N.C.S., 1997, A&A, 318, 187

Crawford D.L., 1975, AJ, 80, 955

Crawford D.L., 1979, AJ, 84, 1858

Drilling J.S., Pesch P., 1973, AJ, 78, 47

Dworetsky, M.M., Moon T.T., 1986, MNRAS, 220, 787

ESA, 1997, The Hipparcos and Tycho Catalogues, ESA SP-1200, ESA Publications Division, Noordwijk

Fehrenbach Ch., Burnage R., Duflot M., Peton A., Rolland L., Genty V., Mannone C., 1987, A&AS, 71, 263

Flower P.J., 1996, ApJ, 469, 355

Giuricin G., Mardirossian F., Mezetti M., 1984, A&A, 134, 365

Grenier S., Baylac M.-O., Rolland L., Burnage R., Arenou F., Briot D., Delmas F., Duflot M., Genty V., Gomez A.E., Halbachs J.-L., Marouard M., Oblak E., Sellier A., 1999, A&AS, 137, 451

Hauck B., 1986, A&AS, 64, 21

Hauck B., Mermilliod J.-C., 1998, A&AS, 129, 431

Hut P., 1981, A&A, 99, 126

Kazarovets A.V., Samus N.N., Durlevich O.V., Frolov M.S., Antipin S.V., Kireeva N.N., Pastukhova E.N., 1999, Information bulletin on variable stars (Commissions 27 and 42 of the IAU), 4659

Kitamura M., Kondo M., 1978, Ap&SS, 56, 341

Lucke P.B., 1978, A&A, 64, 367

Lucy L.B., Sweeney M.A., 1971, AJ, 76, 544

Meynet G., Mermilliod J.-C., Maeder A., 1993, A&AS, 98, 477

Moon T.T., Dworetsky M.M., 1985, MNRAS, 217, 305

Nadal R., Ginestet N., Carquillat J.-M., Pédoussaut A., 1979, A&AS, 35, 203

Nordström B., Stefanik R.P., Latham D.W., Andersen J., 1997, A&AS, 126, 21

Popper D.M., Etzel P.B., 1981, AJ, 86, 102

Schaller G., Schaerer D., Meynet G., Maeder A., 1992, A&AS, 96, 269

Schmidt-Kaler Th., 1982, in Landolt-Börnstein, Numerical Data and Functional Relationships in Science and Technology, K. Schaifers & H.H. Voigt eds., New Series, Gr. VI, Vol. 2-b (Springer-Verlag, Berlin), pp 1–35 and 449–456

Slettabak A., Nassau J.J., 1959, ApJ, 129, 88

Udry S., Mayor M., Queloz D. 1999, in *Precise Stellar Radial Velocities,* ASP Conferences Ser., 185, 367

Walther M.E., 1949, ApJ, 110, 67

Wilson R.E., Joy A.H., 1950, ApJ 111, 223

Wilson R.E., Devinney E.J., 1971, ApJ 166, 605

Young R.K., 1942, Publ. David Dunlap Obs., 1, 249

Zahn J.-P., 1975, A&A 41, 329

Zahn J.-P., 1977, A&A 57, 383

Zahn J.-P., Bouchet L., 1989, A&A 223, 112

Table 11. Orbital elements of the SB1 systems. In Col. 3, T_0 is the epoch of periastron passage, except for systems with $e = 0$ (circular orbits). In that case T_0 corresponds to the ascending node passage.

Name	P days	T_0 (JD) 2400000+	ω deg.	e	K_1 km.s^{-1}	V_0 km.s^{-1}	$a_1 \sin i$ Gm	$f(m)$ M$_\odot$	$\sigma_{(O-C)}$ km.s^{-1}
HD19342	42.6301	49323.630	–	0.0	26.80	6.16	15.71	0.0853	0.37
	±0.0027	±0.075	–	–	±0.10	±0.07	±0.06	±0.0009	
HD19910	15.41418	49325.46	67.2	0.059	45.77	11.64	9.68	0.1526	0.94
	±0.00022	±0.20	±4.8	±0.005	±0.23	±0.17	±0.05	±0.0024	
HD36360	216.54	49129.1	116.1	0.112	12.37	13.90	36.60	0.0417	0.47
	±0.12	±3.6	±6.2	±0.012	±0.17	±0.11	±0.59	±0.0020	
HD102925	16.43718	49798.439	–	0.0	26.62	-0.89	6.02	0.0322	0.64
	±0.00091	±0.046	–	–	±0.17	±0.12	±0.04	±0.0006	
HD127263	14.23834	50488.062	248.6	0.319	24.87	-14.07	4.62	0.01936	0.42
	±0.00014	±0.035	±0.8	±0.004	±0.11	±0.08	±0.03	±0.00034	
HD138406	25.8513	49792.55	9.8	0.213	10.75	-6.68	3.73	0.00311	0.36
	±0.0011	±0.19	±2.6	±0.010	±0.11	±0.08	±0.05	±0.00012	
HD155714	3.334772	49144.192	–	0.0	6.28	-43.63	0.288	0.000086	0.82
	±0.000055	±0.022	–	–	±0.18	±0.13	±0.008	±0.000007	
HD195692	11.292249	48138.102	–	0.0	39.92	-25.49	6.20	0.0746	0.88
	±0.000081	±0.014	–	–	±0.19	±0.14	±0.03	±0.0011	
HD199360	1.9986874	49640.743	–	0.0	11.74	4.90	0.323	0.000336	0.42
	±0.0000086	±0.005	–	–	±0.11	±0.07	±0.003	±0.000009	

Table 12. Orbital elements of the SB2 system of our sample. In Col. 3, T_0 is the epoch of the ascending node passage.

Name	P days	T_0 (JD) 2400000+	ω deg.	e	K_1 km.s^{-1}	K_2 km.s^{-1}	V_0 km.s^{-1}	$a_1 \sin i$ Gm	$a_2 \sin i$ Gm	$M_1 \sin^3 i$ M$_\odot$	$M_2 \sin^3 i$ M$_\odot$	$\sigma_{1(O-C)}$ km.s^{-1}	$\sigma_{2(O-C)}$ km.s^{-1}
HD126031	3.782624	50480.328	–	0.	82.23	110.10	-28.37	4.277	5.727	1.600	1.195	0.92	0.49
	±0.000006	±0.003	–	–	±0.18	±0.26	±0.12	±0.009	±0.014	±0.011	±0.008		

Table 13. Strömgren photometry and derived data with Crawford (1979)'s calibration (see Sect. 4.1).

HD	β	$b-y$	$E(b-y)$	m_1	$(m_1)_0$	c_1	$(c_1)_0$	$(\delta m_1)_0$
19342	2.73	0.31	0.10	0.20	0.23	0.77	0.75	-0.05
19910	2.81	0.19	0.04	0.20	0.21	0.73	0.72	-0.01
36360	2.80	0.16	0.01	0.24	0.24	0.81	0.81	-0.04
126031	2.74	0.20	−0.01	0.23	0.23	0.66	0.67	-0.04
127263	2.83	0.14	−0.01	0.28	0.28	0.80	0.80	-0.07
155714	(2.72)	0.23	0.01	0.19	0.19	0.68	0.67	-0.01
195692	(2.78)	0.16	0.00	0.21	0.21	0.76	0.76	-0.01
199360	(2.81)	0.18	0.03	0.25	0.26	0.74	0.73	-0.06

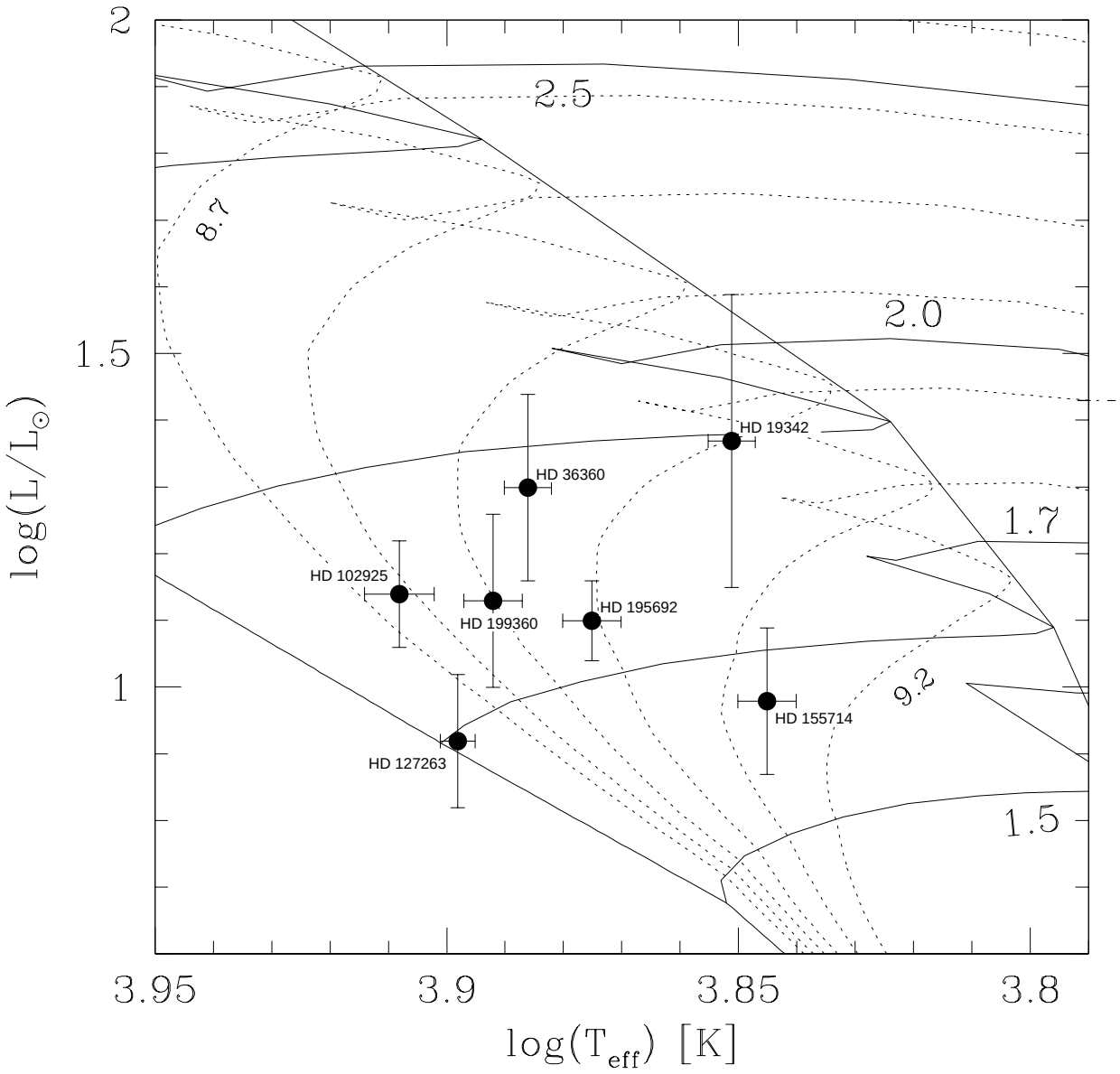

Figure 3. Location of the primary components of the Am SB1 in the theoretical evolutionary HR diagram computed by Schaller et al. (1992) for $Z = 0.02$, with the isochrones (dotted lines) given by Meynet et al. (1993), for log age[years] varying from 8.7 to 9.2 by steps of 0.1. The solid lines correspond to the evolution tracks for mass values of 1.5, 1.7, 2.0 and 2.5 $M_{\odot}$.

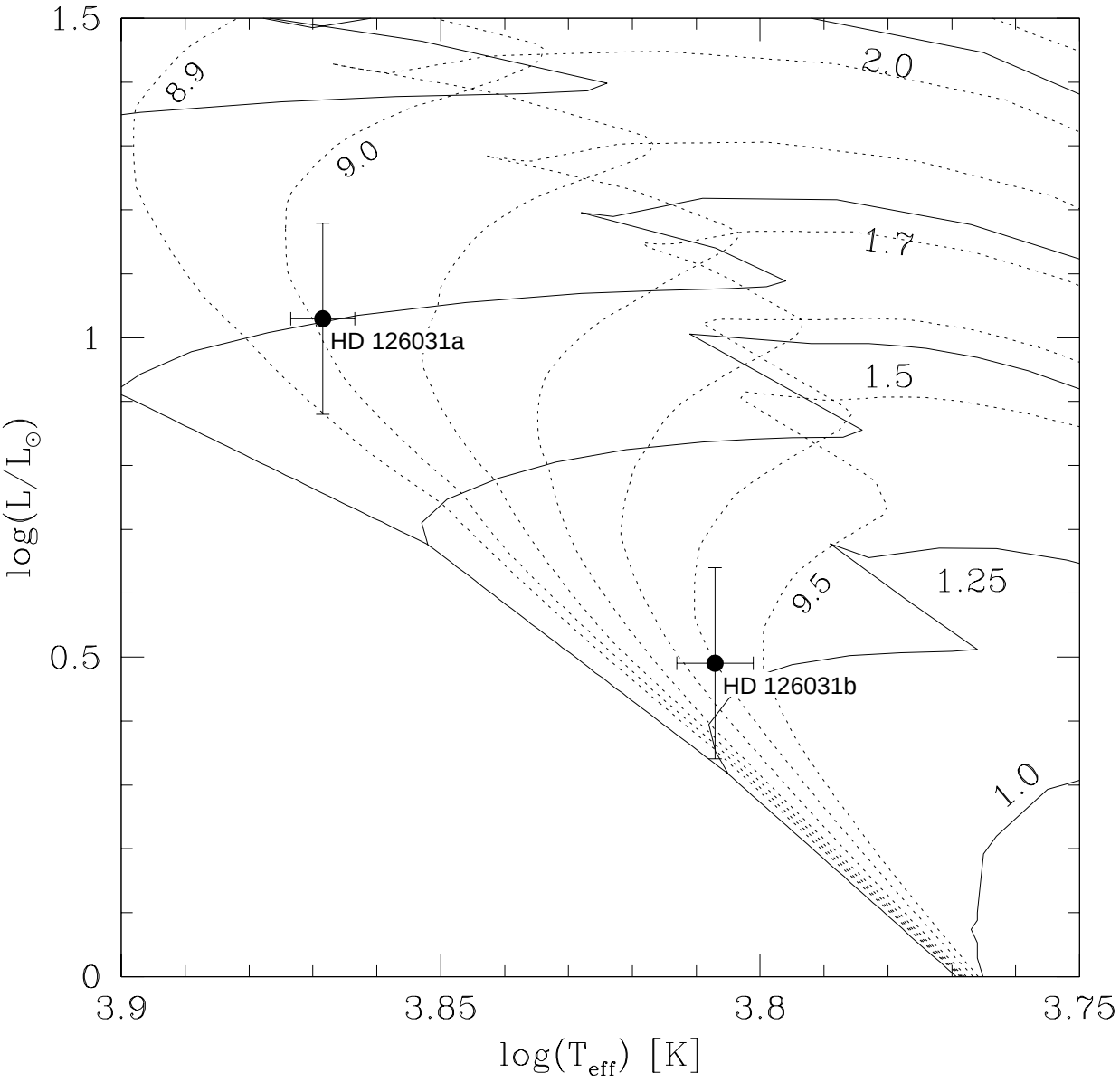

Figure 4. Location of the two components of HD 126031 in the theoretical evolutionary HR diagram computed by Schaller et al. (1992) for $Z = 0.02$, with the isochrones (dotted lines) given by Meynet et al. (1993) (shifted version of Fig. 3).

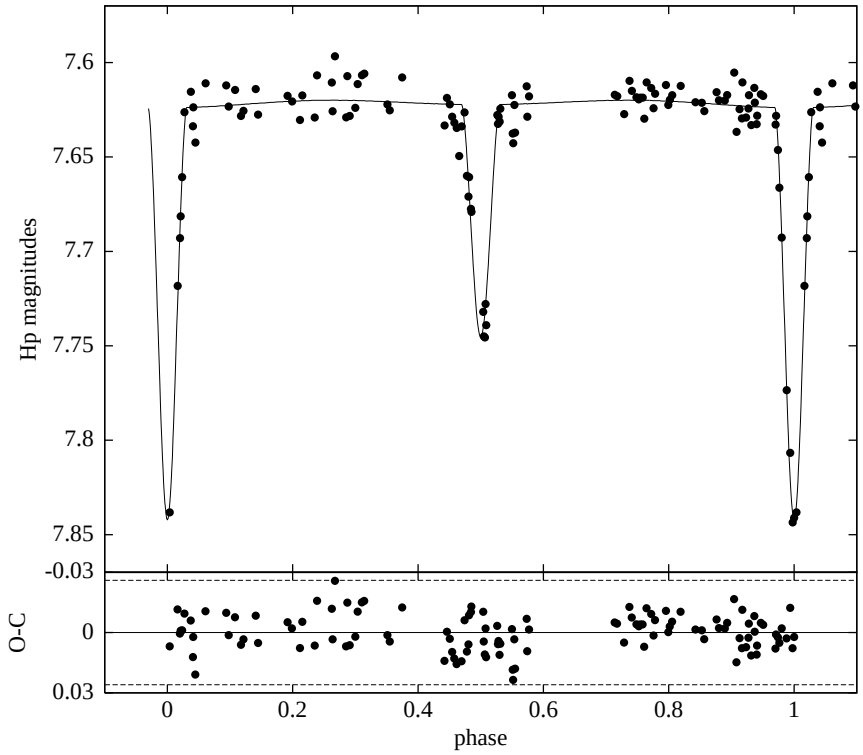

Figure 5. Light curve of HD 126031 obtained by Hipparcos, rescaled to the spectroscopic period, with Min I = HJD 2447859.9071±0.0005 as the origin of phases. The fitted model with EBOP and WD are plotted in solid line and the residuals are given in the bottom with the 3-sigma level marked with dotted lines.

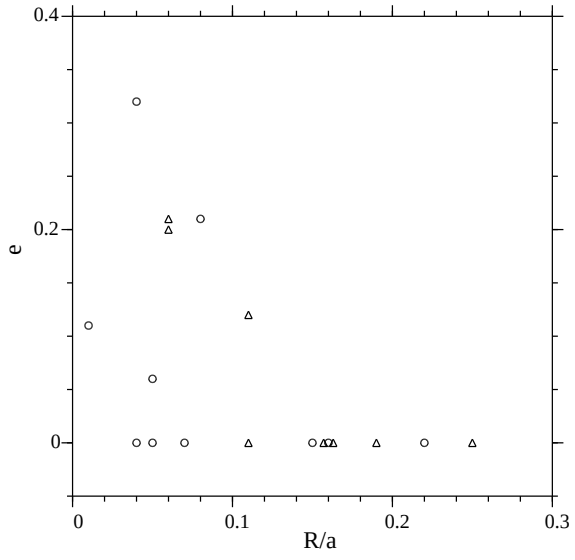

Figure 6. Eccentricity versus the fractional radius R/a for this sample (circles) and for the systems of Paper V (triangles).

Table 14. Estimated physical parameters of the primary components from observational data and theoretical statements. For the reddened objects, the magnitudes corrected for interstellar absorption are indicated in brackets (lines 3 and 4).

HD	19342	19910	36360	102925	126031	127263	138406	155714	195692	199360
HIP	14653	–	25995	57813	70287	70814	75764	84230	101300	103335
V	8.00 (7.59)	9.34 (9.19)	7.17	7.24 (7.14)	7.54	8.14	6.91 (6.74)	7.06	6.51	7.85 (7.73)
$B-V$	0.47 (0.33)	0.30 (0.25)	0.28	0.18 (0.15)	0.34	0.24	0.13 (0.07)	0.38	0.26	0.31 (0.27)
$v \sin i$ (km.s^{-1})	9.9 $\pm$1.0	14.1 $\pm$1.0	20.0 $\pm$1.0	8.0 $\pm$1.0	24.4 $\pm$2.4	11.0 $\pm$1.0	6.6 $\pm$1.0	17.4 $\pm$1.0	9.6 $\pm$1.0	13.5 $\pm$1.0
π (mas)	5.52 $\pm$1.11	–	7.29 $\pm$1.08	8.78 $\pm$0.64	7.38 $\pm$0.92	7.14 $\pm$0.74	3.55 $\pm$0.54	11.06 $\pm$1.21	12.33 $\pm$0.70	6.78 $\pm$0.90
d (pc)	181^{+46}_{-30}	–	137^{+24}_{-18}	114^{+9}_{-8}	135^{+20}_{-15}	140^{+16}_{-13}	282^{+50}_{-38}	90^{+12}_{-9}	81^{+5}_{-4}	147^{+23}_{-17}
M_v	1.30 $\pm$0.51	–	1.48 $\pm$0.32	1.86 $\pm$0.16	2.14 $\pm$0.3	2.41 $\pm$0.23	-0.51 $\pm$0.36	2.28 $\pm$0.24	1.96 $\pm$0.13	1.89 $\pm$0.29
$\log L/L_\odot$	1.37 $\pm$0.22	–	1.30 $\pm$0.14	1.14 $\pm$0.08	1.03 $\pm$0.15	0.92 $\pm$0.10	2.09 $\pm$0.16	0.98 $\pm$0.11	1.10 $\pm$0.06	1.13 $\pm$0.13
T_{eff} (K)	7100 $\pm$70	7800 $\pm$70	7700 $\pm$70	8100 $\pm$100	7370 $\pm$80	7900 $\pm$70	8700 $\pm$150	7000 $\pm$80	7500 $\pm$80	7800 $\pm$80
$\log g$(cgs)	3.6	4.4	4.0	–	4.1	4.1	–	4.0	4.1	4.2
$[Fe/H]$	+0.67	+0.29	+0.55	–	+0.64	+0.93	–	+0.34	+0.30	+0.75
$R_1/R_\odot$	3.2 $\pm$0.8	$\sim$2	2.5 $\pm$0.4	1.9 $\pm$0.2	2.1 $\pm$0.3	1.5 $\pm$0.2	4.9 $\pm$1.0	2.1 $\pm$0.3	2.1 $\pm$0.2	2.0 $\pm$0.4
$M_1/M_\odot$	2.00 $\pm$0.20	$\sim$2.0	1.95 $\pm$0.10	1.85 $\pm$0.05	1.70 $\pm$0.10	1.70 $\pm$0.05	$\sim$ 3	1.65 $\pm$0.10	1.80 $\pm$0.05	1.80 $\pm$0.10
$M_{2\,\min}/M_\odot$	0.9	1.1	0.7	0.6	–	0.4	0.3	0.06	0.3	0.1
$M_{2\,\max}/M_\odot$	1.2	1.2	1.2	1.1	–	1.0	1.8	1.0	1.1	1.1
$a_{\min}/R_\odot$	73.1	38.2	209	36.5	14.5	31.8	54.8	11.2	28.8	8.3
$a_{\max}/R_\odot$	75.6	38.4	222	39.0	–	34.5	61.9	13.0	29.8	9.5
$\overline{a}$	74.4	38.3	216	37.8	14.5	33.2	58.4	12.1	29.3	8.9
$R/\overline{a}$	0.04	0.05	0.01	0.05	0.13	0.05	0.08	0.17	0.07	0.22
$i_{\min}$ (deg.)	53	75	39	36	–	31	13	5	53	7
$R_{\mathrm{sync,min}}/R_\odot$	8.3 $\pm$0.8	4.3 $\pm$0.3	79.6 $\pm$4.0	2.6 $\pm$0.3	1.8 $\pm$0.2	1.9 $\pm$0.2	2.6 $\pm$0.4	1.15 $\pm$0.07	2.1 $\pm$0.2	0.53 $\pm$0.04
Synchronized?	no	no	no	no	yes	$\sim$likely	likely	likely	likely	likely
Circularized?	yes	no	no	yes	yes	no	no	yes	yes	yes
log age[years]	$9.00^{+0.10}_{-0.08}$	–	$8.94^{+0.02}_{-0.03}$	$8.77^{+0.06}_{-0.12}$	$9.00^{+0.03}_{-0.10}$	$\sim 8 \pm 0.7$	$\sim$8.7	$9.13^{+0.03}_{-0.02}$	$9.00^{+0.02}_{-0.05}$	$8.90^{+0.03}_{-0.14}$
$\log t_{circ}$[years]	17.6	16.3	23.4	16.7	12.3	17.2	14.1	11.4	15.4	9.9
$\log t_{sync}$[years]	14.1	12.9	18.7	13.3	9.6	13.7	11.1	9.1	12.2	7.8

Table 15. Results from the fit of the Hipparcos light curve of HD 126031.

Parameter	Value	Error	Unit	Origin
i	82.7	0.3	°	light curve
T_{eff1}	7370	80	K	Strömgren's photometry
T_{eff1}/T_{eff2}	0.87	0.01	–	light curve
R_1	1.94	0.03	$R_\odot$	light curve & spectro.
R_2	1.39	0.04	$R_\odot$	light curve & spectro.
a	14.49	0.01	$R_\odot$	light curve & spectro.
M_1	1.64	0.02	$M_\odot$	light curve & spectro.
M_2	1.23	0.02	$M_\odot$	light curve & spectro.
Δm_V	1.41	0.15	mag.	light curve & spectro